AAS 05-378

STABILITY MAPS, GLOBAL DYNAMICS AND TRANSFERS

Benjamin Villac[*], **Martín Lara**[†]

Homoclinic and heteroclinic connections associated with unstable periodic orbits structure the global transport phenomena in phase space. From a spacecraft trajectory design viewpoint, these connections correspond to thrust-free, dynamical transfers relating, potentially, distant regions of phase space. Stability maps based on a fast Lyapunov indicator are shown to exhibit the main connections of a class of unstable periodic orbits lying at the boundary of stability regions in the planar circular restricted three-body problem. The corresponding transfers are shown to present good recovery properties and may thus form the basic building blocks for some trajectory design problems in planet-satellite systems. The graphical representation of these global dynamics thus enable a quick overview of possible transfer path between different dynamical regimes. These ideas are illustrated in the Jupiter-Europa system.

INTRODUCTION

Dynamical system theory has proven useful for trajectory design and analysis of recent and currently proposed mission [1, 2, 3, 4]. It allowed new classes of transfers to be analyzed and shed some light on the dynamical structures influencing these dynamics. The main methodology for designing such transfers is based on the use of unstable periodic orbits (u.p.o) and their associated manifolds to find thrust-free transfer arcs between different regions of phase space.

While these dynamical transfers are very attractive from a fuel budget viewpoint, these transfers present, however, several difficulties. Aside from the well studied case

[*]Member of the engineering staff, Guidance, Navigation and Control section, Jet Propulsion Laboratory,California Institute of Technology, M/S 301-140L, 4800 Oak Grove Drive, CA 91109, Benjamin.F.Villac@jpl.nasa.gov

[†]Commander, Ephemeris Department, Real Observatorio de la Armada, 11110 San Fernando, Spain, mlara@roa.es

of the libration point dynamics, the choice of the source/target u.p.o. needs trial and errors, and systematic trade-offs between different classes of u.p.o. do not seem available. The current understanding comes from the notion of resonance region, where the u.p.o. of lowest period, appearing when invariant tori of quasi-periodic orbits are destructed, seem to govern the transport in and out of the resonance region. This is particularly true in the 2D case where resonances can be defined as regions of phase space bounded by branches of stable/unstable manifolds of such u.p.o.. The spatial problem is more complex as multiple u.p.o. associated with a given resonance generally exist and have to be taken into account. The separation property of the manifolds, that holds in the 2-dimensional case, fails in the spatial problem. The computation and choice of such u.p.o. for a particular purpose thus represents a difficult task.

A second concern generally associated with these dynamical transfers are the strong sensitivity with respect to the initial conditions, and thus, the sense of instability associated with these transfers. While the Soho and Genesis mission have demonstrated that such trajectories can be flown in the Earth-Moon-Sun system [1, 5], it remains true that the instability of such transfers may become a challenge when it comes to systems such as the Europa-Jupiter system, where the instability time scale is now on the orders of days, rather than month or year in the Earth-Moon-Sun system.

However, these dynamical transfers may present remarkable recovery properties. For example, since these transfers consist of long coast arcs converging toward an u.p.o., a low-thrust powered transfer that would lie near such manifolds at each instant of time during the transfer would present predictable coast arcs _ the manifold _ without any impact/escape risk on any major body for a period of time, in the event of loss of power. Thus, while immersed in a chaotic sea, some of these transfer would seem very interesting even for missions with strong planetary protections requirements.

While this recovery property exist in theory, the target of very unstable u.p.o. reduces its effectiveness, as a particle would converge and depart from the u.p.o. too quickly to allow for an acceptable error margin or recovery time. The target of higher order u.p.o., however, provides a solution to this problem, as the guaranteed coasting arcs are now much longer and the instability time scale can also be longer. The location of the particular u.p.o. is related to their proximity with stability island formed by sets of stable, quasi-periodic orbits which can be detected using chaoticity indicators [6].

This paper aims at discussing how chaoticity indicators (via the use of the Fast Lyapunov Indicator, or FLI), can be helpful in analyzing the above issues. In particular, the use of stability maps allows us to place the transfers into context, relating u.p.o. to the nearby stability islands, and thus indicate possible initial conditions

that lead to more stable transfers.

Note that, while the complete design of a high-fidelity trajectory proceeds generally in two distinct steps:

- computation of the desired transfer based on the choice of u.p.o. in a simplified system, such as the Circular Restricted Three-Body problem.
- differential correction to adapt the initial transfer estimate to a more realistic model (e.g., ephemeris)

only the first step requires some knowledge of the global dynamics of the system and appears as the most challenging part in the design. Our discussion will focus on this first step and will use the planar circular restricted three-body problem (PCR3BP) to illustrate the ideas.

After reviewing the dynamical background associated with these transfers, a discussion of FLI maps, their relation to periodic orbits and their potential uses is presented. These ideas are then illustrated by the computation and analysis of several examples of such transfers.

UNSTABLE PERIODIC ORBITS AND TRANSFERS

This section quickly reviews the basic dynamics underpinning of dynamical transfers and discuss interesting recovery properties of such transfers. While the dynamical background can be found in many references (see [8, 9] for example), we were not able to find a reference discussing the recovery properties of these dynamics for spacecraft applications after a brief literature search.

Unstable periodic orbits and their manifolds

The nature of a periodic orbit is determined by analyzing the eigen-structure of the monodromy matrix associated with any state along the given orbit. The monodromy matrix, M, is the state transition matrix evaluated after one complete period, T, of the periodic orbit. Therefore, it captures the linearized dynamics of the flow sampled every T instant of time. A periodic orbit is stable when the monodromy matrix possesses an eigenvalue or characteristic multiplier, λ greater than one.

Indeed, the state resulting from a small perturbation δu_o from a state x_o on the periodic orbit will be mapped after one period to the state $x_o + M.\delta u_o$. If one of the eigen-values has modulus greater than one, a small perturbation in the direction of the corresponding eigen-vector, will result in an increase in the perturbation after one period: $M.\delta u_o = \lambda \delta u_o$, so that $||M.\delta u_o|| > ||\delta u_o||$. Moreover, as the perturbation $M.\delta u_o$ lies also in the same direction as u_o, in the linear approximation to the dynamics, the set of initial conditions perturbed in the direction of this unstable eigen-direction from the initial state x_o forms a 1-dimensional subspace, which, after

propagation in time, results in a 2-dimensional linear manifold, the (linear) unstable manifold associated with the periodic orbit.

Now, In the autonomous hamiltonian framework of the model considered (PCR3BP), the state transition matrix associated with the linearized dynamics around any solution is symplectic, so that its eigen-values come in reciprocal/complex-conjugate pairs or quadruples. Thus, the existence of an unstable eigen-values λ, $|\lambda| > 1$, of the monodromy matrix implies the existence of a corresponding "stable" eigen-values, λ', $|\lambda'| = 1/|\lambda| < 1$, and a corresponding stable eigen-direction and (linear) stable manifold. Any initial condition lying on this stable manifold will converge towards the initial periodic orbit as time increases. The phase portrait of these saddle dynamics is illustrated in Figure 1. Thus stable and unstable manifolds corresponds to the contracting and expanding subspaces in the vicinity of an u.p.o.

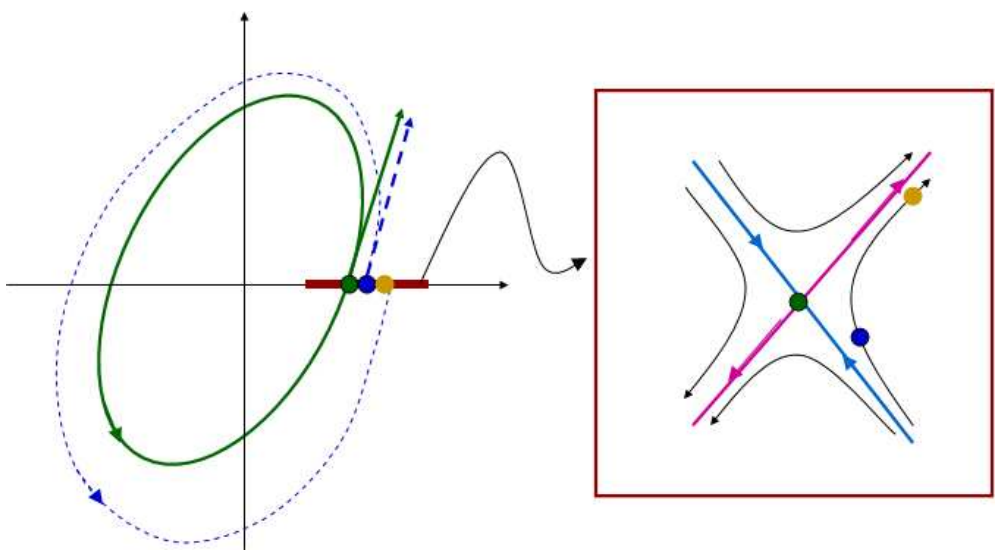

Figure 1: Cartoon representing the saddle dynamics appearing on a surface of section (red), that results from an unstable periodic orbit (green). The light blue and pink lines on the right plot, represent the cross-section of the stable and unstable manifolds of the u.p.o., respectively..

A classical theorem in dynamical systems [8, 9], guarantees that this linear picture is preserved in the actual dynamics of the original system. The linear manifolds obtained from the linear analysis now exist as smooth 2-dimensional manifolds embedded in the energy manifold*.

Thus, an unstable manifold, denoted $W^u(u_0)$, is smooth set of trajectories which converge towards the u.p.o., u_o, as time goes to $-\infty$. Similarly, a stable manifold,

*In our autonomous hamiltonian framework, the hamiltonian function defines a first integral of motion and the set of initial conditions resulting in a given value for the hamiltonian form a sooth manifold of codimension one in phase space. This manifold is called the energy manifold.

denoted $W^s(u_o)$, is a smooth set of trajectories which converge towards u_o as time goes to $+\infty$.

Finally, we note that the above linear analysis provides a simple tool to numerically approximate the manifolds of an u.p.o., once a state on the u.p.o. and its period are known.

Manifolds and transfers

While, in general, the manifold W^u and W^s do not coincide (as sets of points in phase space), they often intersect and the trajectories lying in such intersections converge towards the corresponding u.p.o. as time goes toward both $+\infty$ and $-\infty$. These particular trajectories are called homoclinic connections.

Whereas a transfer from a periodic orbit back to the same periodic orbit does not seem of immediate utility, the general case of a transfer between two different u.p.o. is certainly useful. For example, the one of the legs of the trajectory of the Genesis mission approximated a dynamical transfer relating two different halo orbits [1], one near the libration point $L1$ of the Earth-Sun system, and the other, near the corresponding L_2 point.

Trajectories lying in the intersection of an unstable manifold of a u.p.o., u_1, and a stable manifold of a u.p.o., u_2, are called heteroclinic connections. They depart the neighborhood of the first u.p.o.[†], and converge towards the second u.p.o. as time goes to $+\infty$.

Thus, it appears that in non-integrable systems, such as the CR3BP, where manifolds of different u.p.o. intersects, "thrust-free' transfers are possible and present a potential class of transfers for current and future space missions. The design of such transfers relies on the knowledge of a source and target u.p.o. (and possibly intermediary u.p.o., as well), their associated manifolds and connections.

Trade-offs and design

As noted in the introduction the design and implementation of dynamical transfers present several difficulties:

- The set of u.p.o. in phase space is very large and a choice of the source and target u.p.o. for some design problem is not clear.
- If analyzed over a sufficiently long time, the unstable dynamics associated with these transfers present a high sensitivity with respect to the initial conditions.

While the first difficulty can be addressed by placing the different periodic orbits into context (next section), the second difficulty represents, in fact, a trade-off be-

[†]Assuming that both u.p.o., do not lie in the same neighborhood.

tween time scale and sensitivity, complementing the ΔV *v.s.* time-of-flight trade-off considered in [10].

Indeed,while the above dynamics are the backbones of chaotic motion[‡] and, thus, result in high sensitivity with respect to the initial conditions, these phenomena involve the consideration of the flow over relatively long time spans. The motion near a given u.p.o. and for short enough time spans, is a smooth deformation of the linear dynamics which present a certain recovery property that may be of interest for trajectory design that requires to take into account the potential failure of the engines during maneuvers that would stay at each instant of time along such manifolds.

In order to illustrate our point, we consider the archetypical system corresponding to the normalized linear picture of the saddle dynamics around a u.p.o. on a Poincaré surface of section:

$$\begin{pmatrix} x_{n+1} \\ y_{n+1} \end{pmatrix} = \begin{pmatrix} \lambda & 0 \\ 0 & \frac{1}{\lambda} \end{pmatrix} . \begin{pmatrix} x_n \\ y_n \end{pmatrix} \quad \text{with} \quad \lambda \in \mathcal{R}, \lambda > 1$$

The stable manifold branches of this system are given by the positive and negative y-axis, while the x-axis corresponds to the unstable manifold. The general solution of this system is easily seen to be $(x_n = \lambda^n x_0, y_n = \lambda^{-n} x_0)$, so that the hyperbolic relation, $x_n y_n = x_0 y_0$, holds.

Now, requiring a spacecraft to be in a neighborhood of size ϵ at a given time $n > 0$, results in constraining x_0 and y_0 to satisfy the relation:

$$x_0 . y_0 < \epsilon^2 \quad \text{or, assuming, } y_0 > 0, \quad x_0 < \frac{\epsilon^2}{y_0} \tag{1}$$

This condition shows a trade-off between the initial distance from the u.p.o. and the closeness of the initial state from the stable manifold to reach the u.p.o. within a certain accuracy. The farther away from the u.p.o. the spacecraft initially lies, the closest it must be from the stable manifold.

In practice, the accuracy on the knowledge of the state of a spacecraft is not infinite and the upper bound on x_0 cannot be taken arbitrarily small. Thus, let us assume that the state can only be known to within an accuracy δ. Using the previous constraint, we see that the largest distance that a spacecraft can be from the u.p.o. in order to reach it within ϵ is constrained by:

$$y_0 < \frac{\epsilon^2}{\delta} \tag{2}$$

For example, a positional accuracy δ of 1 km and a requirement to meet an u.p.o. within 100km results in requiring the spacecraft to lie within 1 km of the stable manifold at a distance no greater than $10,000$km. Note that these estimates are only

[‡]Chaotic motion is, by definition, the nature of the flow in the neighborhood of connections [8, 9].

given here to illustrate our point. Even in simple models, such as the PCR3BP, The manifold of an u.p.o. are curvy so that the path length along the manifold is not directly related to the distance from the u.p.o., and far away from the u.p.o., the non-linear effects are certainly of importance. However, the above argument shows that, depending on the constraints imposed on the trajectory, the targeting of a stable manifold can be performed from some distance to the final u.p.o., while still ensuring convergence towards the approximate target for some time span.

While the knowledge of the path length from the current state to the target may be of interest, recovery properties during maneuvers are generally stated in terms of time requirements. For example, one can imagine a spacecraft performing a low-thrust transfer and encountering a hardware malfunction that would results in the loss of thrust capability for some period of time. Assuming that such a transfer lie within δ of the stable manifold of some u.p.o., what would be the time span allowed by the dynamics before the spacecraft would embark upon an undesirable path from which the recovery of the nominal path may be difficult to perform?

While the above path length constraints do not depend on the characteristic multiplier of the u.p.o., the above problem does involve the time scale of the problem, and u.p.o. with a mild instability will result in larger recovery time (at constant fundamental period) than a highly unstable periodic orbit. Indeed, using our simplified saddle dynamics, we can see that an ϵ-neighborhood of the u.p.o. stretches apart along the unstable directions, so that an uncertain state in this neighborhood will have equal probability in going along either branch of the unstable manifold (i.e., the positive or negative x-axis in the example chosen). When dealing with actual spacecraft trajectories, this may mean being ballistically captured or not by a planetary satellite, as for example in the dynamics associated with the libration points [ref]. Thus, the recovery time allowed by the dynamics is less than the time taken to travel from the current state along the stable manifold to the ϵ-neighborhood around the u.p.o.

From the previous equations, we easily see that the recovery time n is thus bounded by the following relation:

$$n < \frac{\log \epsilon/\delta}{\log \lambda} \tag{3}$$

The smaller the characteristic multiplier of the u.p.o., the longest the recovery time. For example, assuming again that $\delta = 1$km, $\epsilon = 100$km, the recovery time for $\lambda = 1.5$ is ~ 11 time units, while it is only 2 and 1 time units for a λ value of 10 and 100, respectively. Note that in the simple dynamics considered to illustrate the trade-off between recovery time and characteristic multiplier, the fundamental period of the u.p.o. does not enter, as the saddle dynamics considered is based on the monodromy matrix analysis. However, recalling the definition of this matrix, one immediately see that the unit time of the problem are in fact set as this fundamental period. Thus, a λ value of 1.5 would result in approaching the periodic orbit in 11 fundamental periods. The longest this period, the longest the recovery time.

STABILITY MAPS AND CONNECTIONS

From the previous discussion, we have seen that the design of dynamical transfers rely on the computation of u.p.o. and their manifolds. However, as we pointed out, the number of u.p.o. is large and not every connection seem suitable for designing transfers, due mostly to the too high sensitivity of some of these transfers or the too lengthy time of flight required.

From a design viewpoint, the knowledge of a single trajectory meeting some given requirements is generally not sufficient as changes in policy, funding, or the event of a missed maneuver result in a modification of the requirements and back-up options or alternatives are often sought for. Thus placing trajectory into their dynamical context may help future trajectory designer in answering some of these challenges more efficiently. Stability maps present one tool that may help in this endeavor.

Stability maps

In a range of energy near that of the libration points, the phase space of the PCR3BP is a mixture of regular and chaotic motion. Regular motion, or stable periodic and quasi-periodic motion, tends to group into small clusters forming regions of long-term stability. While tiny chaotic layers may still exist in these region, the approximate, numerical distinction of chaotic and regular motion using chaoticity indicators can seem sufficient to locate such stability regions [6, 7]. The time scale used for these computations is indeed finite and the tiny chaotic layers appear as regular motion at these time scales.

The fast Lyapunov indicator (FLI) is a chaoticity indicator based on the expansion properties of the state transition matrix that allows for a quick separation of strongly chaotic motion from regular trajectories [11]. While several definition have been used in the literature, we use the definition adopted in [6] with a normalizing factor based on the current state, so as to obtain a scale invariant indicator.

$$FLI_n(T) = \sup_{i,t \leq T} [\log ||\delta u_i(t)||_n] \tag{4}$$

where $\{\delta u_i\}$ represents the state at time t of the evolution of a basis of initial perturbation vectors. The evolution of these perturbations is obtained by integrating the first variational equations. Noting that a small perturbation vector can be split into a position and velocity part, $\delta u = (\delta r, \delta v)$, the norm $||\delta u||_n$ is defined as $\sqrt{(||\delta r||/r)^2 + (||\delta v||/v)^2}$, where $||.||$ is the usual Euclidean norm and r and v are the magnitude of the position and velocity at the current state of the spacecraft. The use of this metric thus results in a scale invariant definition of the FLI. The time scale, T, entering the definition of the FLI has been taken to be 628 normalized units in the PCR3BP, which represents a time span of about 100 periods of Europa around Jupiter.

By computing the FLI for a set of initial conditions and representing the index

value as a density map over the chosen set, one obtains stability maps indicating the different stability islands intersecting the set of initial conditions considered. For example, Figure 2 represents an FLI map in the PCR3BP modeling the Jupiter-Europa system. The initial condition plane considered corresponds to trajectories crossing the x-axis with $\dot{y} > 0$ at a fixed Jacobi constant of $C = 3.0$. From this picture, one can see the existence of a large chaotic sea (higher values of the FLI, orange-yellow color on the picture) and the different stability islands associated with distant retrograde motion around Europa and resonant motion around Jupiter (lowest values of the FLI, purple color). Other Stability maps can be found for example, in [6, 7].

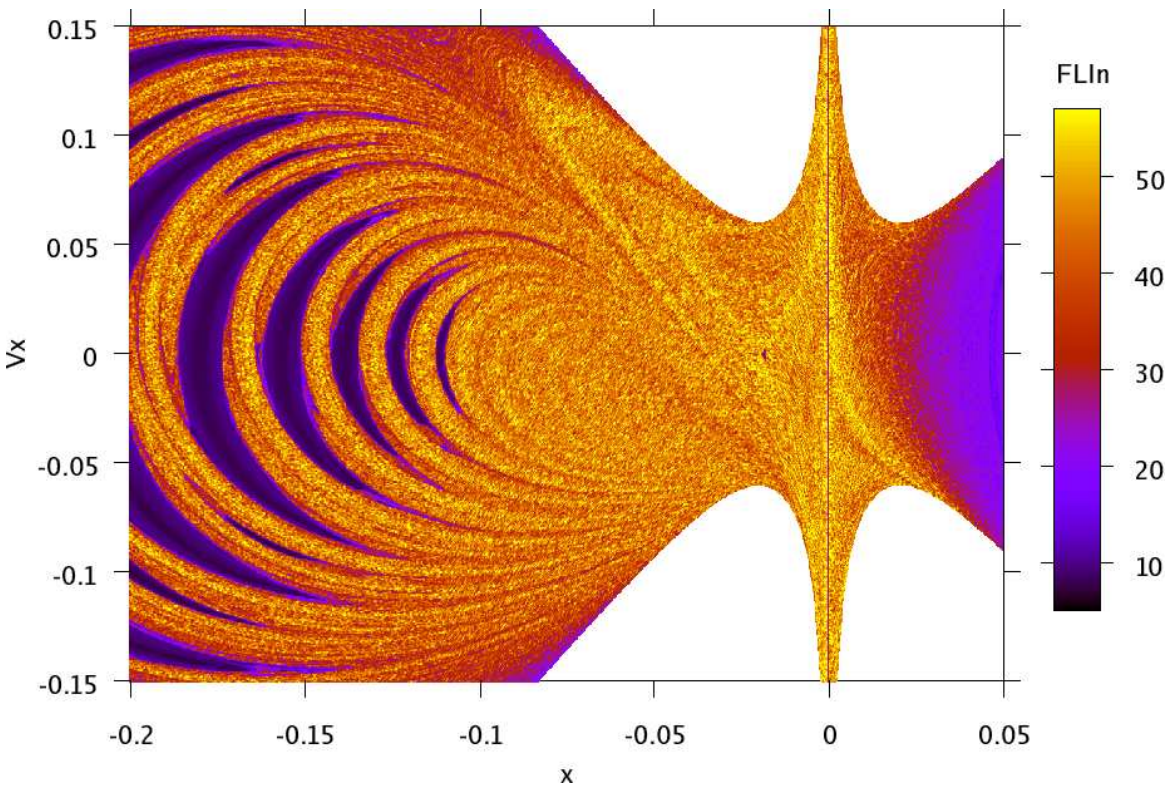

Figure 2: Example of an FLI map in the Jupiter-Europa system modeled by the PCR3BP with $\mu = 2.528 \times 10^{-5}$ at a Jacobi constant of $C = 3.0$.

Relation to periodic orbits

The transition from regular motion near the boundary of the stability regions is structured by the presence of u.p.o., which correspond to members of families of periodic orbits bifurcating from some stable family in the stability island under consideration [7].

For example, one can find simple periodic orbits near the center of each croissant shaped stability island in the previous maps. Starting from the smaller island located

around $x \simeq -1.1$, the series of simple periodic orbits orbits for the successive first four islands are presented in Figure 3.

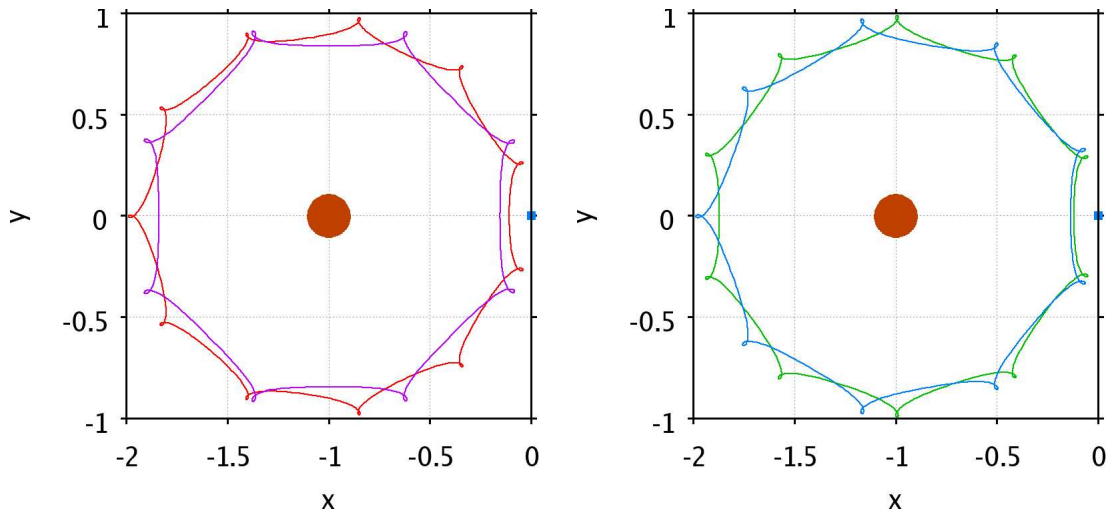

Figure 3: (a) Resonances 11:10 (red) and 8:7 (purple) (b) Resonances 10:9 (green) and 9:8 (blue). Jupiter is represented as a marron disc and Europa as a blue square.

Note that these periodic orbits make about 11, 10, 9, and 8 complete revolutions around Jupiter, while Europa completes, 10, 9, 8 and 7 orbits, respectively. We will thus refer to these stability islands as the 11:10, 10:9, 9:8 and 8:7 resonant isalnd, respectively.

Now, as the Jacobi constant varies, the shape and size of the stability islands vary [7] and the central periodic orbit may bifurcate with some families of unstable periodic orbits. At these points, the size of the stability region surrounding these simple periodic orbits disappear (at least in the planar case). This is what have been observed by several researchers for the case of the distant retrograde orbits (DRO) [14, 6, 13], leading the a weakening of the strong stability of these orbits, known as the "neck region". The bifurcation of the DRO familiy in the planar case occurs through a period tripling bifurcation and the corresponding family of periodic orbits lie at the boundary of the stability region assocaited with the DRO family for C values away from these bifurcation points.

Similarly, by plotting the linear stability indices of the period 10 family of orbits of whom one member has been presented in Fig. 3(b), another period tripling bifurcation occurs at $C = 2.98745$. In the same manner, as for the DRO case, this family "sticks" to the boundary of the 10:9 stability resonant island, and turns out to correspond to one of the most influencing periodic orbit for transfers relating to this resonant island. Figure 4 presents the linear stability indices of these families and the period tripling bifurcation point. The corresponding critical orbit is also shown on that Figure.

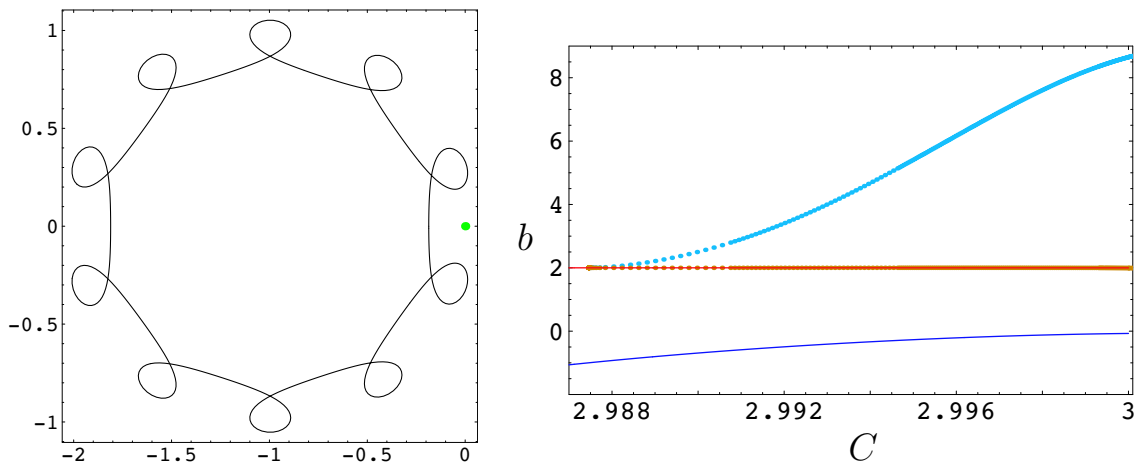

(a) (b)

Figure 4: (a) Shape of the periodic orbit of the 10:9 family at the period tripling bifurcation point (Europa represented as a green dot). (b) Horizontal, linear stability indices of the 10:9 periodic orbits family (dark blue) and the triple period, bifurcating , unstable family (light blue). The orange curve represents the vertical stability index of the 10:9 stability. It is very close to, but smaller than 2.

These boundary unstable periodic orbits, or b.u.p.o., thus play a a fundamental role for transfers using stability islands as source or target. They are generally associated with some kink in the boundary of the stability region and are thus, rather easily recognizable given an FLI map of sufficient resolution. If the information of the bifurcation diagram of the family under consideration is not available (or that one is only interested in a quick overview of the dynamics at a particular Jaocbi constant value), the use of a differential corrector to refine the initial conditions of the b.u.p.o. read from the FLI map is a quick and conveninent tool to explore the dynamics. Aside, from these main bifurcations, many b.u.p.o. of higher period exist and correspond to the transition in stability properties of some families of periodic orbits of long period lying in the stability island considered[§]. These b.u.p.o. tends to have a lesser influence on the dynamics that concerns us, as their time scale is very long.

Stability maps and manifolds

Besides indicating the location of some u.p.o., the stability maps reveal some structures in the chaotic sea. Indeed, looking back at the above map (Fig. 2), one can observe small variations in the FLI values in the chaotic sea forming 1-dimensional curves. Notably, some of these curves emanate from the vicinity of the location of

[§]These "higher order" periodic orbits also appear as bifurcations from the fundamental periodic orbit.

the b.u.p.o. and the superimposition of the intersection of their manifolds with the slices of initial conditions corresponding to these stability maps confirm indeed that these particular structures do correspond to the trace of the manifolds associated with these b.u.p.o. For example, Fig. 5 presents such an operation for the unstable, planar DRO and one can clearly attest of the match.

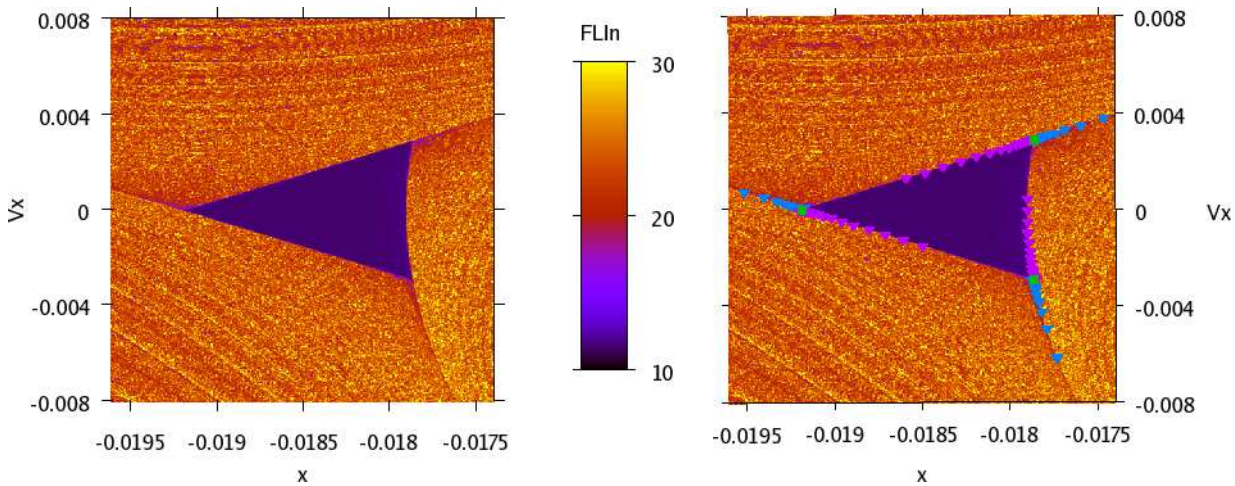

(a) (b)

Figure 5: (a) Forward FLI map around a distant retrograde orbit (magnification of the small stability dot, "lost" in the chaotic sea of Fig. 2 between $x = -0.05$ and $x = 0.0$); (b) with b.u.p.o. initial conditions (green squares) and stable manifold branches overlaid (blue and pink triangles).

These features appear more apparent as the integration time in the FLI computation time is not taken to be too long and reflects the fact that the initial conditions lying near the stable manifold linger around for some time before getting caught and being scattered away by the unstable manifolds. Thus if the integration time is not too long, the stretching in the immediate negihborhood of the stable manifold will be less than for an initial condition lying a little further away. As the time increases, the width over which this effect can be observed shrink and the curvy lines approximating the stable manifold in the FLI computation are less pronounced. Thus we used half the time adopted in the creation of the first map of this paper (Fig. 2) to generate the previous two maps (Fig. 5) and the maps that follows in the paper.

Similarly, unstable manifolds present the same contraction property as the stable manifolds, when one considers the dynamics in backward time. Thus, it is to be expected that the computation of stability maps in backward time would reveal the trace of the unstable manifolds of the b.u.p.o. This is illustrate on Fig. 6 which presents the same set of initial condition as in Fig. 5, but with a backward computation of the FLI. As for Fig. 5, the unstable manifold of the boundary unstable DRO is superimposed, showing again the good agreement between the structures revealed by the FLI computations and the unstable manifold.

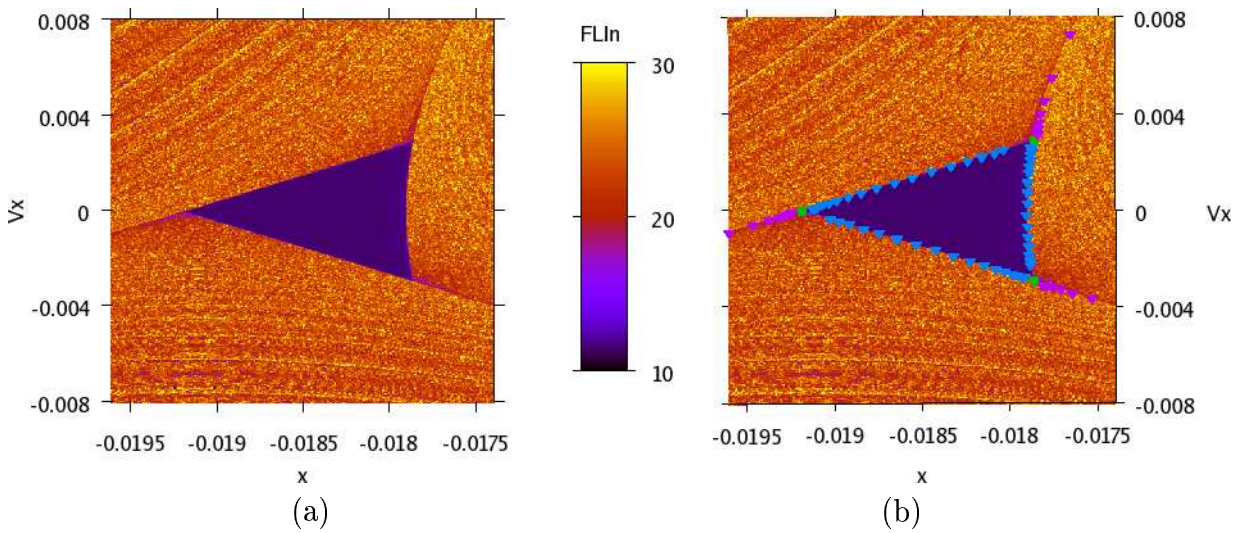

Figure 6: (a) Backward FLI map around a distant retrograde orbit; (b) with b.u.p.o. initial conditions (green squares) and unstable manifold branches overlaid (blue and pink triangles).

Thus, the computation of backward and forward maps indicates the evolution of the unstable and stable manifolds associated with the b.u.p.o., without computing either the corresponding periodic orbit or the manifolds themselves. As the heuristic argument and the examination of several stability maps showed, the trace of the these manifolds is the more apparent, the smaller the characteristic exponents are small.

Forward/backward maps and connections

We have seen that connections are the result of the intersection of stable and unstable manifolds associated with some u.p.o.. Thus, by superimposing two stability maps, one computed in forward time and the other computed in backward time, the main connections between the different b.u.p.o. appears. This superimposition can be performed in several manner, and the method chosen here, consist in computing the mean value of the FLI associated with an initial conditions. That is, if FLI^+ denote the FLI value when computed using forward integration, and FLI^- the FLI value obtained with backward integration, we define the mean FLI as:

$$FLI_m = \frac{1}{2}\left(FLI^+ + FLI^-\right) \tag{5}$$

Applied on the previous case of the stability region around the DRO at $C = 3$, one obtains Fig. 7 where both the stable and unstable manifolds are visible directly on the map. More globally, Fig. 8 and 9 show the stability maps computed on a larger scale, showing the different connections present between the different resonant

island. These connections appear as intersections of the traces of the manifolds associated with the different b.u.p.o.. Once can, for example, observe the pronounced connections between the 9:8 and 10:9 stability islands (primary intersection point at $x \sim -0.0921, \dot{x} \sim 0.0553$) and the 7:8 and the 8:7 islands (primary intersection point at $x \sim -0.0980, \dot{x} \sim 0.0805$. Note that the resonant island tends to regroup in pair, with similar positioning of the even/odd numerators of the resonance relations.

Note also on Fig. 9 the lobe structures associated with the connections that govern the transport phenomena involving the resonance region [12]. We can also appreciate on this Figure, the benefit of using the mean value of the FLI, as the location of the b.u.p.o. are much more easy to distinguish: b.u.p.o. lie at the 'x' shapes near the boundary of the stability islands.

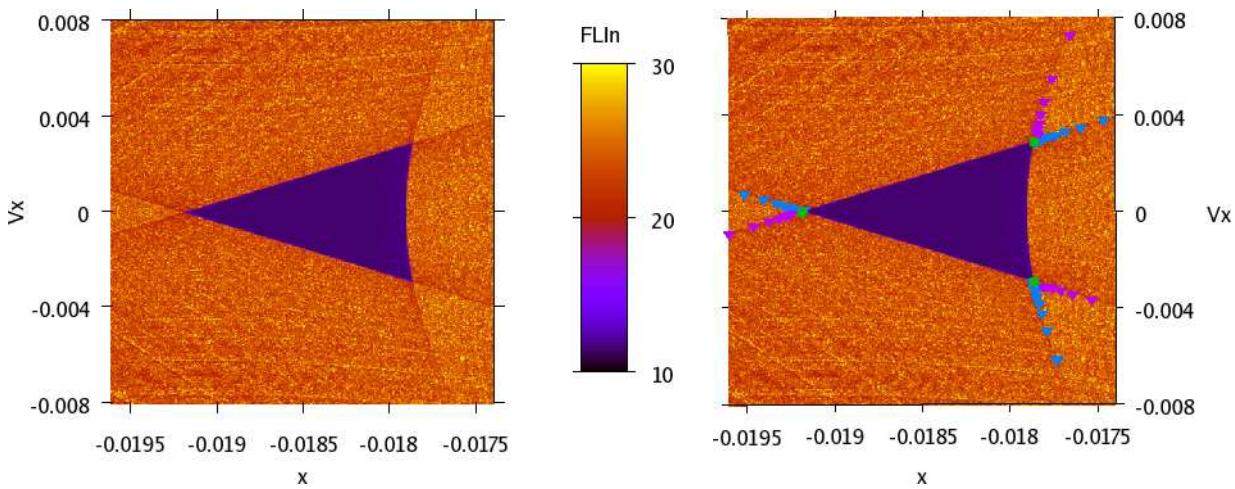

(a) (b)

Figure 7: (a) Mean FLI map around a distant retrograde orbit; (b) with b.u.p.o. initial conditions (green squares) and associated manifolds overlaid (blue triangles: stable manifold branch; pink triangles: unstable branch).

Note that in the problem considered, PCR3BP, the time reversal symmetries can be used to obtain the forward/backward time knowing only the forward map. Indeed, if $(x(t), y(t), \dot{x}(t), \dot{y}(t), t)$ represents a solution of the equations of motion of the PCR3BP, it is a simple matter of substitution to check that $(x(-t), -y(-t), -\dot{x}(-t), \dot{y}(-t), -t)$ and $(-x(-t), y(-t), \dot{x}(-t), -\dot{y}(-t), -t)$ are also solutions of these equations. These discrete symmetries also hold for the variational equations, so that the forward FLI value on an initial condition of the form $(x_o, 0, \dot{x}_o, \dot{y}_o)$ is the same as the backward FLI value for the initial condition $(x_o, 0, -\dot{x}_o, y_o)$. A similar situation holds for the initial conditions of the form $(0, y_o, \dot{x}_o, \dot{y}_o)$ and $(0, y_o, \dot{x}_o, -\dot{y}_o)$, respectively. Thus, on the initial condition plane defined by the conditions, $x = 0$ and $\dot{y} > 0$ (or $y = 0$ and $\dot{x} > 0$, for e.g.), computing the forward FLI maps and performing simple

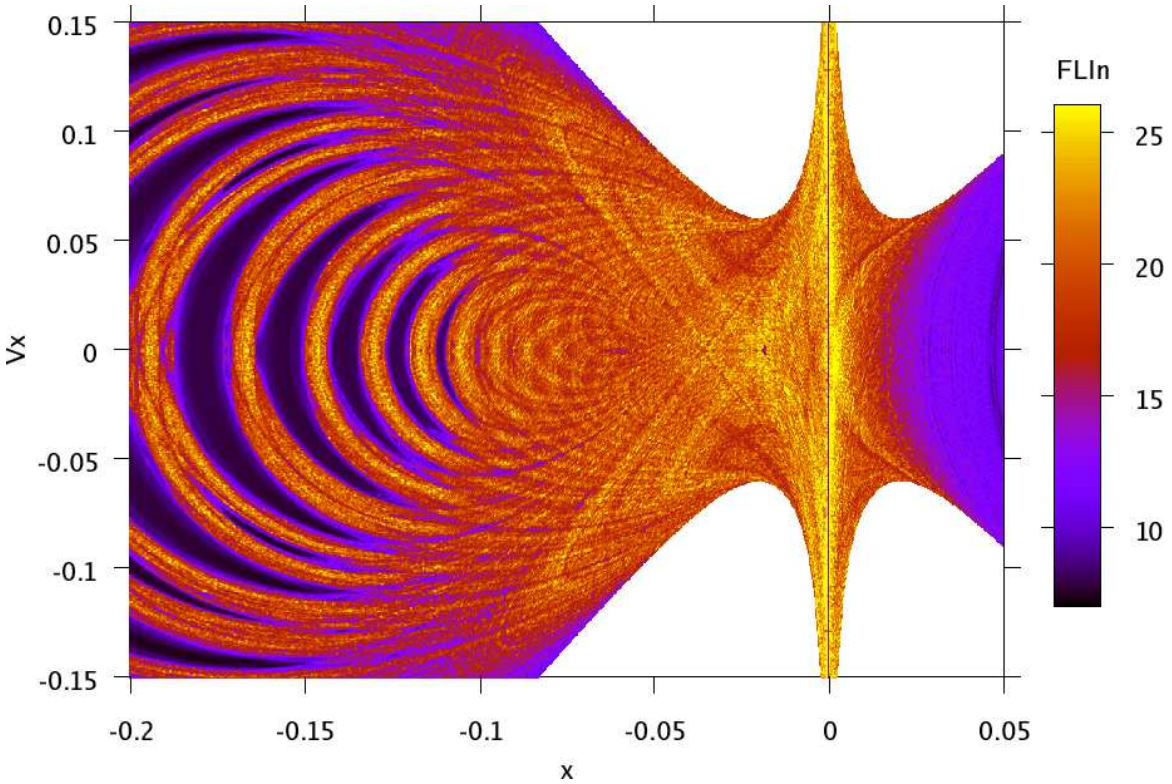

Figure 8: Mean FLI map corresponding to the case shown in Fig. 2.

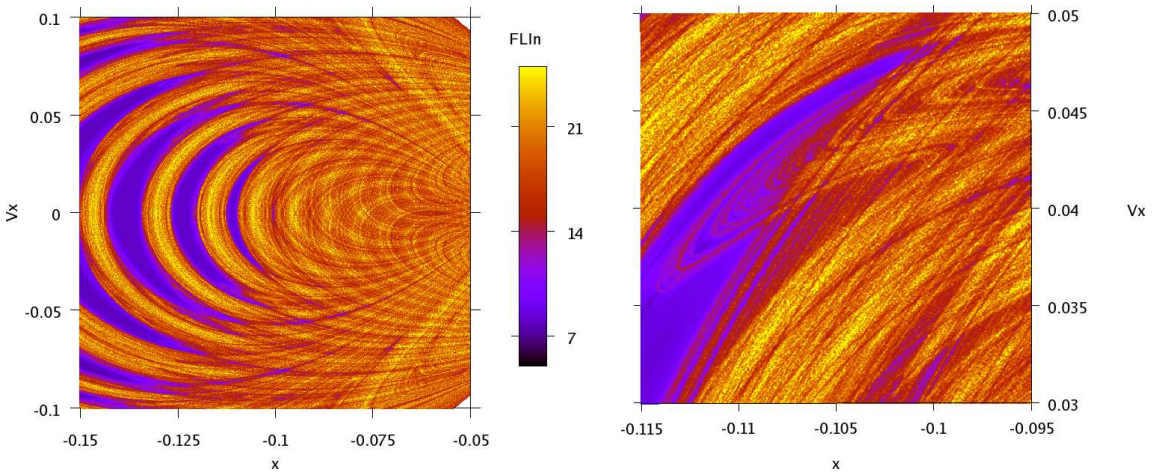

(a) (b)

Figure 9: Mean FLI map corresponding zoomed regions of Fig. 8.

data operations on the resulting file, suffices to generate the corresponding mean FLI maps.

Finally, note that the computation of and FLI in forward time and backward time for half the value of a given time span T is overall equivalent to computing the FLI values for the whole time span. Looking back to Fig. 7, one can observe that the features in the chaotic sea are indeed less apparent, as would be if a forward map using an integration twice as the one used for generating Fig 5(a). Thus, the use of symmetries in conjunction with the choice of the initial condition plane can result in decreasing the computaional cost of the map generation by two. The resulting maps are in fact more interesting with all regards, as the mean value of the FLI does reveal the stability island features more sharply. This is due to the smoothing of the lingering effect of the trajectories near the stable manifolds for forward maps (and unstable manifolds for backward maps), resulting in seemingly elongated streches of the stability regions. By computing the mean FLI value, this lowerig value of the FLI is uniformized, without eleiminating the structures appearing in the chaotic sea.

TRANSFER EXAMPLES

As we have seen in the background section, connections are synonyms with thrust-free transfers legs. The mean FLI maps, thus allow us to obtain a quick overview of the possible transfers between different regions of phase space. Moreover, the knowledge of the nearby stability islands indicates the expected type of motion to be enountered in the vicinity of the source and target u.p.o., thus placing these transfers into their dynamical context.

Transfer between two resonant islands

To illustrate how the dynamical maps obtained can be used for a transfer design, we consider the case of a to transfer of a spacecraft from the boundary of the 10:9 resonant island, towards another resonance region. While the two main connections pointed out in the previous section would result in such a transfer, the changes in orbital elements (relative to Jupiter) would seem to be small.

By scrutinizing more closely the mean FLI map of Figs. 8 and 9, one can see that some orange lines emanating from the 10:9 resonant island intersects another such line that emanates from the 8:7 resonant island. An approximate initial condition for this intersection point can be read[¶] from Fig 8: $x = -0.076$; $\dot{x} = -0.0613$ (at $y = 0$, $C = 3.0$). While this initial condition only approximate the actual connections present in this model, Generating a zoom around this point allows us to refine the initial condition for this connection, as shown in Fig. 10(a). Using the reading

[¶] The reading is done via the pointer of a mouse on a computer. The coordinate of the mouse pointer automatically reflects its position on the graph, so it is easy to get fairly accurate readings quickly.

$x = -0.0764766$ and $\dot{x} = 0.0618624$, one obtains the transfer shown on Figs. 10(b) and 11.

As we can see the backward integration of the initial condition obtained from the FLI map results in a converging trajectory towards the source u.p.o., represented in red on Fig 11(b) and corresponding to the member of the period-tripling bifurcated familie at $C = 3.0$. We note, that this b.u.p.o. is in an approximate 30:26 resonance with Europa, very close from the approximate 10:9 relation of the simple periodic orbit lying at the center of the resonance island. The forward integration of the initial condition does also lead to the desired resonance region, resulting in a change in periapsis radius of about 0.05 normalized unit, or $\sim 33,500$ km. Note, however, that the transfer time is rather large $\sim$ 1.5 year, thus illustrating the important trade-off between time-of-flight and the use of mildly unstable dynamical pathways.

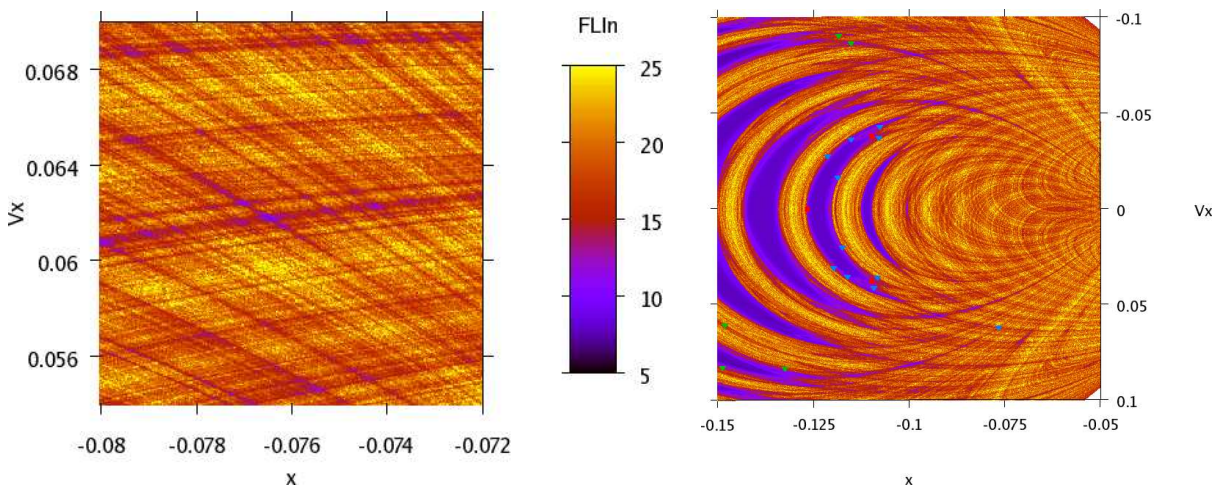

(a) (b)

Figure 10: (a) Mean FLI map near a connection point relating the 10:9 and 8:7 resonance regions. The connection point is naturally emphasized by a low FLI value. (b) Corresponding transfer viewed on the surface of section $y = 0$ and $\dot{y} > 0$.

Transfer between an unstable DRO and a resonant island

The refinement of the above initial conditions for the transfer can be alternatively obtained by computing the unstable manifolds of the source b.u.p.o., the stable manifolds of the target b.u.p.o. and their natural intersections. The FLI maps helps us in this case by indicating that the desired connection does indeed exist. This manifold computation method does seem, however, necessary when close fly-bys result in too much stereching for the features present in the chaotic sea to remain apparent (scattering).

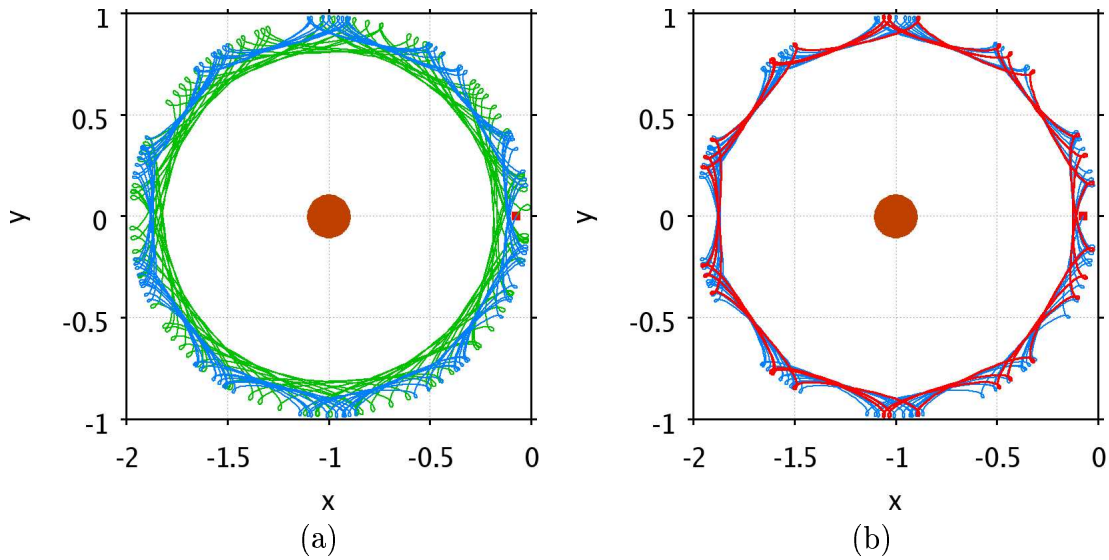

Figure 11: (a) Transfer representation on position space. The red square corresponds to the connection point, the green leg represents the forward integration in time, while the blue leg represents the backward integration. (b) backward leg (blue) with the source periodic orbit. Jupiter is represented by the marroon disc centered at $(-1, 0)$.

For example, in order to compute a transfer between an unstable DRO and a b.u.p.o., the unstable manifold of the unstable DRO is first computed and the intersection with the stable manifold associated with the target b.u.p.o. is then obtained via the FLI maps method[‖].

Note that, as opposed to the previous transfer example, this transfer (not shown) involves a large change in sem-major axis, which results from the presence of a fly-by after the departure form the DRO region. This example is typocal of a DRO type capture/escape [4].

This brief description of this transfer is here to show that both the map and manifold computations can be complementary. A comprehensive appraoch using a variety of tools seem to be the most esffivcient way of dealing with difficult questions regarding these complex dynamics.

CONCLUSIONS AND FUTURE DIRECTIONS

An illustration of the potential use of chaoticity indicators based on the state transition matrix has been presented. By placing the transfers into a dynamical context, the maps may help a mission trajectory designer in analyzing potential alternative trajectories from a reference trajectory. The recovery properties of transfers targetting mildly unstable periodic orbits have also been discussed from an heuristically

[‖] Alternatively, one can also computate the stable manifold of the target b.u.p.o..

viewpoint and related to the existence of nearby stability islands.

While only thrust-free transfer legs have been discussed in this paper, the ideas and tools presented here may also be useful to better understand low-thrust transfers from a dynamical viewpoint. This understanding may lead to the efficient generation of good initial guesses to input in optimizers. This problem is intimately related on the chaining of several coast arcs by using simple control laws near the unstable periodic orbit. A future paper will aim at discussing these issues. Another direction of study should also aim at extending the ideas presented in this paper to the 3-dimensional problem, which would illustrate more fully the advantage of using chaoticity indicators to partially reduce the dynamics on initial condition planes.These methods may also be useful for designing resonant fly-by and analyze the trade-offs present between the inter-moon transfers in orbital environment such as the Jupiter-Galilean moon system.

Finally, we should like to point out that further investigations of other types of indices for transfer analysis purposes would be of interest. For example, chaoticity indicator based on the frequency analysis of spacecraft trajectories may present certain advantages, as they do not require, for example, the integration of the variational equations of the system.

ACKNOWLEDGEMENTS

Part of this work has been performed at the Jet Propulsion Laboratory , California Institute of Technology, under a contract with the National Aeronautics and Space Administration. Martín Lara acknowledges partial support from the Spanish Government (project numbers ESP2004-04376 and ESP-2005-07107).

References

[1] Lo, M.W., Williams, B.G., Bollman, W.E., Han, D., Hahn, Y., Bell, J.L., Hirst, E.A., Corwin, R.A., Hong, P.E., Howell, K.C.,"Genesis Mission Design", Paper AIAA 1998-4468, AIAA/AAS Astrodynamics Specialist Conference and Exhibit, Boston, MA, Aug. 10-12, 1998.

[2] Gómez, G, Llibre, J., Martinéz, R., Simó, C., "Dynamics and Mission Design Near Libration Points", Vol. I, World Scientific Pub., Co., Singapore, 2000.

[3] Find other reference by Kathy Howell, ...

[4] Whiffen, G., "A Preliminary Investigation of the Jupiter Icy Moon Orbiter", AAS paper 03-354, presented at the 2003 AAS/AIAA Astrodynamics Specialists Conference, Big Sky, Montana.

[5] Find a reference on the Shoh mission or the IEEE-7 mission.

[6] Villac, B.F., Aiello, J., "Mapping Long-term stability regions using the Fast Lyapunov Indicator", paper AAS 05-188, presented at the 15th Spaceflight Mechanics Meetings, Copper Mountain, Colorado, January 2005.

[7] Villac, B.F., Lara, M., "On parking solutions around Europa", paper AAS 05-384, to be presented at the 2005 AAS/AIAA Astrodynamics Specialists Conference, Lake Tahoe, California.

[8] Wiggins, S. *Introduction to applied nonlinear dynamical systems and chaos*, Texts in applied mathematics, Vol. 2, Springer-Verlag, 1990.

[9] , Ott, *Introduction to Choas*, Cambridge University Press, 1998.

[10] Ross, S.D., Koon, W.S., Lo, M.W., Marsden, J.E., "Design of multi-moon orbiter", Paper AAS03-143, 2003 AAS/AIAA Space Flight Mechanics Meeting, Ponce, Puerto Rico.

[11] Froeschle, C., Lega, E., "Fast Lyapunov Inidcators. Application to Asteroidal Motion.", *Celestial Mechanics and Dynamical Astronomy*, Vol. 67, pp. 41–62, 1997.

[12] Wiggins, S. *Chaotic transport in dynamical systems*, Springer-Velrag, 2000.

[13] Lam, T., Whiffen, G.J., "Exploration of Distant Retrograde Orbits around Europa," paper AAS 05-110, presented at the 15th Spaceflight Mechanics Meetings, Copper Mountain, Colorado, January 2005.

[14] Simo, Stuchhi,"Central stable/unstable manifolds and the destruction of KAM tori in the planar Hill problem", *Physica D*, Vol. 140, No. 1-2, pp. 1-32, 2000.